Microstructure and properties of Cu-TiNi composites prepared by vacuum hot pressing

X. Zhang[a], Z. Xiao[a,b,*], Z. Xia[a], S. Han[a], X.P. Meng[a,c], Y. Y. Zhao[d], Z. Li[a,e], Q. Lei[e]

[a] School of Materials Science and Engineering, Central South University, Changsha 410083, China.

[b] Key Laboratory of Non-Ferrous Metal Materials Science and Engineering, Ministry of Education, Changsha 410083, China.

[c] Ningbo Boway Alloy Material CO., Ltd, Ningbo 315135, China.

[d] School of Engineering, University of Liverpool, Liverpool L69 3GH, UK.

[e] State Key Laboratory of Powder Metallurgy, Central South University, Changsha 410083, China.

Highlights

- TiNi particles are uniformly distributed in the Cu-TiNi composites.
- The diffusion (CuNi)Ti layer formed.
- There is a semi-coherent relationship between the Cu matrix and (CuNi)Ti phase.
- The mechanical property of composites increases by increasing TiNi content.

Abstract

Cu-TiNi composites with TiNi volume percentages of 1%, 5%, 10% and 15% were prepared by vacuum hot pressing and hot extrusion. The microstructure, thermal and mechanical properties of the composites were analyzed. The results show that diffusion of elements occurred at the interface between the Cu matrix and the TiNi particles during the preparation process, leading to the formation of a (CuNi)Ti diffusion layer. The TiNi particles are uniformly distributed in the Cu-TiNi composites, with a well-bonded interface with the Cu matrix. Cu matrix has major <111> + minor <001> fiber textures after hot extrusion. There is a semi-coherent relationship between the Cu matrix and the (CuNi)Ti phase, with an orientation relationship of $(111)_{Cu} \| (103)_{(CuNi)Ti}$ and an angle of 18.7° between the two crystal planes. Both the Vickers hardness and the compressive yield strength of the Cu-TiNi composites increased with increasing the volume percentage of the TiNi particles, while the thermal expansion coefficient showed an opposite trend. The thermal expansion coefficient, Vickers hardness and compressive yield strength of the Cu-15% TiNi composite are 14.11×10^{-6} /K, 154.4 Hv and 460.0 MPa, respectively.

Keywords

Cu-TiNi composite; hot pressing; interface microstructure; mechanical properties

1. Introduction

Copper and its alloys are widely used in the electrical and electronic industries as electrical contact materials, integrated circuit lead frames, contact wires for rail transit and electrodes for resistance welding due to their excellent electrical and thermal properties [1], [2]. The relatively low strength and hardness of pure copper, however, have limited their applications as structural materials [3]. Cu-based composites are often developed for these applications. These composites are usually prepared by adding reinforcing phases, including short or long fibers, whiskers and finely dispersed particles, to improve the mechanical properties. The most common reinforcing materials are ceramics such as SiC and Al_2O_3. When Cu matrix composites are used as electronic packaging materials, carbon materials (such as carbon fibers, diamond particles, carbon nanotubes) and metals (such as tungsten, molybdenum) are often added as reinforcements to reduce their thermal expansion coefficients [4], [5], [6], [7].

In recent years, TiNi shape memory alloys have been used as reinforcements in metal matrices in order to obtain better mechanical and physical properties, including yield strength, fatigue strength, damping and thermal expansion properties. Because of their shape memory effect, super elasticity and high damping properties [8], [9], [10], adding shape memory alloys can not only improve the mechanical properties but also provide some functional properties of the metal matrix composites [11]. Li et al. [12] reported that the Cu-TiNi composites prepared by rolling had a thermal expansion coefficient of 4×10^{-6} /K, which is much lower than that of Cu. Aydogmus et al. [13] prepared a Mg-TiNi composite by electric spark sintering and found that its compressive yield strength and elastic modulus increased with temperature due to stress introduced by phase change. Ahn et al. [14] prepared an Al-TiNi composite by an infiltration method and found its damping capacity to be about 70% of that of the pure TiNi ingot. For metal matrix composites reinforced with a shape memory alloy and deformed in the martensite state of the shape memory alloy, increasing temperature to above the austenite transformation temperature (A_s) can induce the phase transformation of the shape memory alloy. The internal

compressive stress introduced by the associated contraction can significantly increase the tensile strength and fatigue performance and decrease the thermal expansion coefficient of the composites [15], [16], [17]. Above the martensitic transformation start temperature (M_s), the TiNi shape memory alloy can be deformed in the form of stress-induced martensitic transformation rather than slip of dislocations, the dominant deformation mechanism in traditional metallic materials. Because the critical stress of austenite to martensite transformation generally increases with increasing temperature [18], the strength of the TiNi shape memory alloy increases with increasing temperature due to the increased difficulty of the martensitic transformation. This feature makes the TiNi shape memory alloy an ideal reinforcement phase for Cu and Cu alloys.

The interfacial bonding between the metal matrix and the TiNi reinforcement is critical for the mechanical properties of the composites. A well-bonded interface can transfer stress more effectively from the matrix to the TiNi reinforcement. Li et al. [12] discovered a 6 μm thick diffusion layer at the interface in a Cu-TiNi composite prepared by rolling, without identifying its composition. Thorat et al. [19] also found a second phase around the TiNi particles in a Mg-TiNi composite, formed by diffusion. Hu et al. [20] prepared an Al-$TiNi_f$ composite by hot isostatic pressing and found that $TiAl_2$, TiAl and $TiNi_3$ phases existed in the multilayer interface. However, little work has reported to date on the microstructure of the Cu-TiNi interface in Cu-TiNi composites. Tao Xiao et al. [21] fabricated a Cu/TiNi composites through electroless deposited and powder metallurgy, However, the microstructure of Cu matrix and interface between the matrix and TiNi phase were not discussed, which could be crucial for the thermal and mechanical properties of the composites. Besides, the influence of the volume percentage of TiNi on the thermal expansion and mechanical properties of composites was also not reported.

In this article, Cu-TiNi composites with different TiNi contents were prepared by vacuum hot pressing sintering and hot extrusion. Compared with the previous study [21], we simplified the preparation process for Cu-TiNi composites, without losing the comprehensive properties of the composite. The microstructure and properties of Cu-TiNi composites,

especially the orientation relationship between the Cu matrix and the diffusion layer interface, were characterized and analyzed in details. In addition, the influence of the volume percentage of TiNi on the microstructure and properties of the Cu-TiNi composites were also studied. The results could be expected to understand the effect of TiNi powder on the mechanical and physical properties of copper based alloy and guide the production of the composites.

2. Experimental Procedures

The raw materials were a Cu powder (particle size ≤200 mesh, purity ≥99.99%) and a TiNi powder (particle size ≤200 mesh, purity 99.95%, Ti-Ni atomic ratio 47:53), as shown in Fig. 1. The Cu and TiNi alloy powders were mixed with a V-type blender, with the volume percentage of the TiNi alloy powder being 1%, 5%, 10% or 15%. The powder mixture was cold pressed into a compact with radius 20 mm and height 30 mm by a YD32-1500 hydraulic press with a pressure of 50 MPa and a holding time of 2 min. The compact was heated up at a heating rate of 15°C/min and kept at 900°C for 1 h in a vacuum hot pressing machine under vacuum of 10^{-4} Pa (The mechanical pump, Roots pump and diffusion pump of the heat pressing machine make the vacuum in the furnace reach 10^{-4}Pa.). It was hot pressed under a pressure of 20 MPa and then cooled with furnace. The hot-pressed Cu-TiNi compact was finally subjected to hot extrusion at 900°C with an extrusion ratio of 8. The extrusion rate was kept at 4.0 mm/s during the entire extrusion process. Specimens were cut from the hot-extruded Cu-TiNi composite samples for subsequent tests.

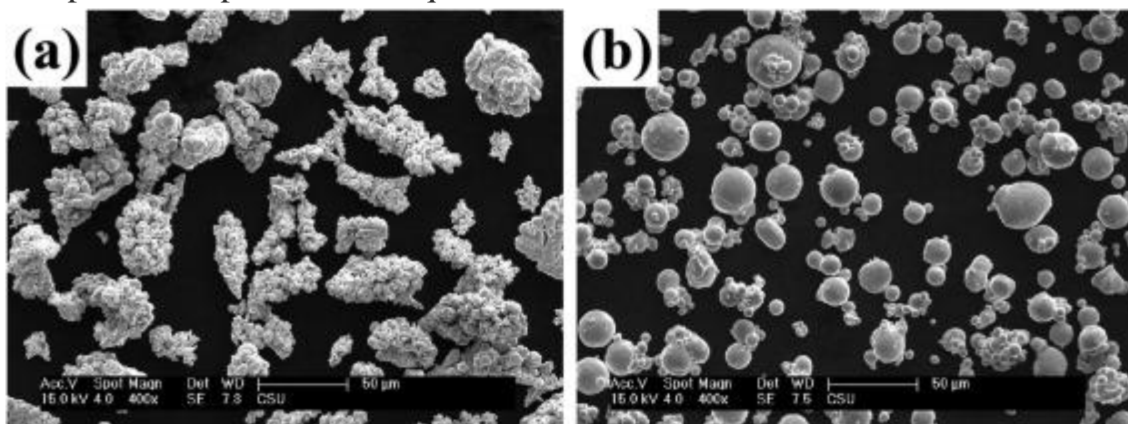

Fig. 1. SEM images of original powders: (a) Cu; (b) TiNi.

The microstructure of the Cu-TiNi composites specimens was observed by a Leica EC3 metallurgical microscope. Microstructure characterization of the Cu matrix was conducted by an FEI Helios Nanolab 600i scanning electron microscope equipped with an Oxfors NordlysMax2 EBSD detector. EBSD samples were prepared by mechanical grinding and polishing followed by electrolytic polishing in a solution of phosphoric acid and ethanol (1:1 vol.%). Electrolytic voltage was kept as 2 V. EBSD data were analyzed through an Oxford instrument HKL technology Channel 5 software. The microstructure of the interface between the Cu and TiNi phases was analyzed by a Titan G2 60-300 transmission electron microscope (TEM). The diffusion in the interface layer was analyzed by a JXA-8230 atom probe microanalyzer. The phase composition was obtained by a Rigaku D/Max 2500X-ray diffractometer. The TEM samples were prepared by Focused Ion beam (FIB).

The microhardness of the Cu-TiNi composite specimens was measured by an HMV-2T micro-Vickers hardness tester, with a test load of 2000 g and the pressure holding time of 10 s. The compressive strength was measured by an MTS-810 fatigue testing machine. The samples for compressive test had a diameter of 8 mm and a height of 12 mm. The thermal expansion coefficient was measured by a thermal dilatometer (DIL 402 C/1/4/7 G).

3. Results and Discussion

3.1. Microstructure of Cu-TiNi composites

The microstructures of the hot-extruded Cu-TiNi composites with different TiNi volume percentages are shown in Fig. 2. There are no discernible pores in the Cu-TiNi composites after hot extrusion, although a small number of TiNi particles show original pore defects (marked by arrows), indicating that the as-prepared Cu-TiNi composites are dense. The TiNi particles are uniformly distributed in the Cu matrix, without any obvious agglomeration. Most TiNi particles remain spherical, showing no significant plastic deformation.

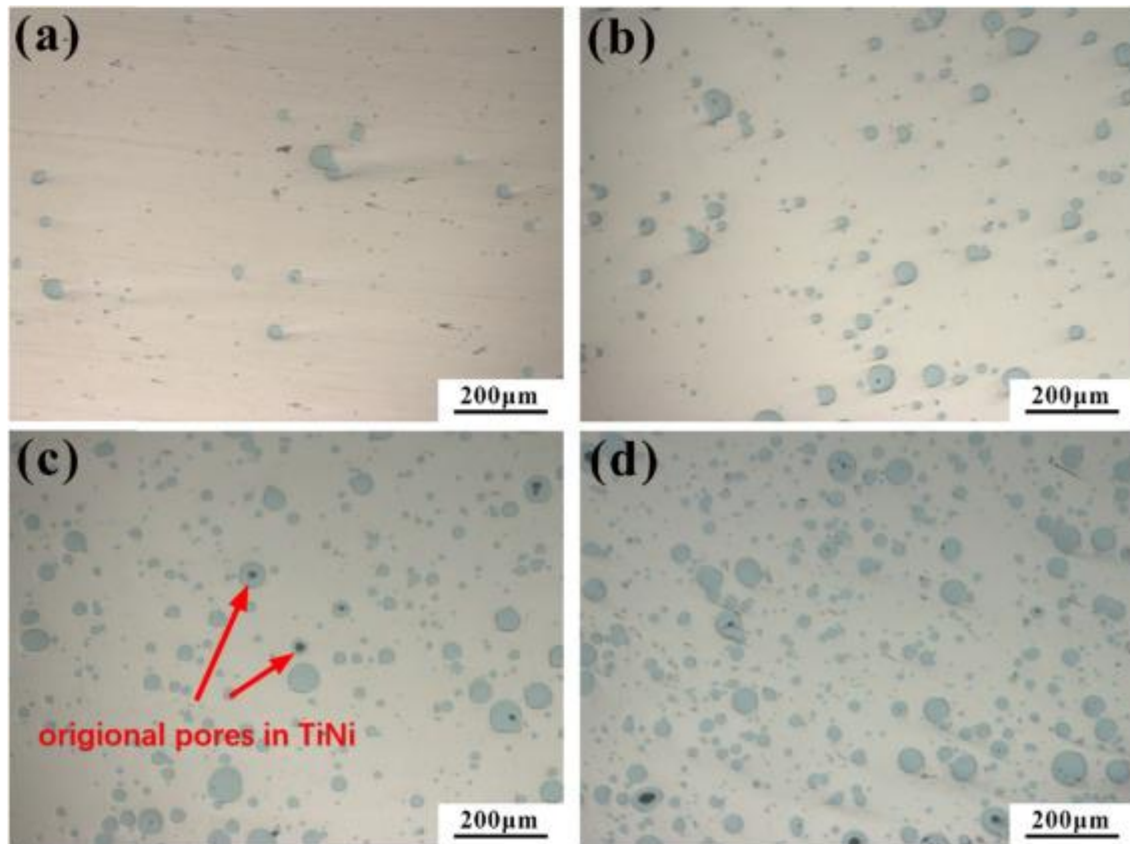

Fig. 2. Microstructures of extruded Cu-TiNi composites with different TiNi volume percentages: (a) 1%; (b) 5%; (c) 10%; (d) 15%.

The SEM image of a typical TiNi particle in the 15 vol% TiNi composite and its distribution of elements are shown in Fig. 3. A significant contrast exists between the center and edge of the TiNi particle (Fig. 3a), indicating different compositions of the two regions. The distribution of elements in the interface region between the Cu matrix and the TiNi particle (Fig. 3b) shows that there exists a Cu diffusion layer with a thickness of about 15 μm at the edge of the TiNi particle, which is consistent with the experimental observations by Li et al. [12]. The following observations can be made in the diffusion layer: (1) the concentration of Ti remains largely unchanged and does not vary with the distance from the interface; (2) the concentration of Cu decreases gradually with the distance from the interface; (3) the concentration of Ni increases gradually with the distance from the interface.

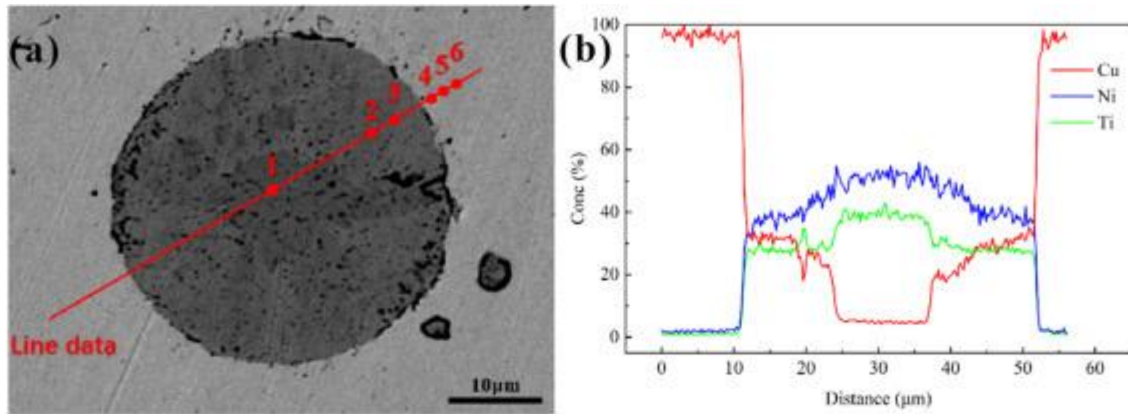

Fig. 3. SEM image and element distribution of TiNi particle in Cu-15% TiNi composite: (a) cross-section; (b) element line analysis of Cu, Ni and Ti.

The concentrations of Cu, Ni and Ti at various spots inside and outside the TiNi particle shown in Fig. 3(a) are shown in Table 1. In the center of the TiNi particle, the concentrations of Ti and Ni basically remain the same and there is a small amount of Cu, which is consistent with the line scan results in Fig. 3. In the diffusion layer, the Ti concentration remains unchanged while the Cu and Ni concentrations vary with the distance from the interface, with Ti accounting for about 1/3 and Cu and Ni totaling about 2/3. The elemental analysis of the interface region between the Cu matrix and the TiNi particle shows that the diffusion of Cu atoms during hot pressing and hot extrusion is the dominant factor for the formation of the diffusion layer. This result agrees with that reported by Luo et al. [22] in their study into the diffusion mechanism in the interface region formed in explosive welding of TiNi shape memory alloy to Cu.

Table 1. Concentrations of elements at various spots inside and outside the TiNi particle shown in Fig. 3(a).

Element	Spot 1	Spot 2	Spot 3	Spot 4	Spot 5	Spot 6
Ni (at%)	48.30	41.90	37.80	1.32	1.22	1.14
Ti (at%)	48.40	36.20	35.20	1.43	1.40	1.08
Cu (at%)	3.30	21.90	27.00	97.25	97.38	97.78

Mohri et al. [23] studied the diffusion of Cu in a TiNi shape memory alloy with the B2 structure and reported that the diffusion coefficient of Cu in the Ni-rich TiNi alloy follows the Arrhenius function as follows, with a pre-

exponential factor of $5.8\pm1\times10^{-14}$ m^2/s and an activation energy of 40±4 kJ/mol:

$$D = 5.8 \pm 1 \times 10^{-14} \exp\left(\frac{-40\pm4kj/mol}{RT}\right) m^2/s \qquad (1)$$

where R is the molar gas constant and T is thermodynamic temperature.

There are several diffusion mechanisms in B2 (CsCl-type) intermetallic compounds: six-jump-cycle, triple-defect, anti-structure-bridge and vacancy-pair [23]. The six-jump-cycle mechanism usually occurs in compounds with high ordered stoichiometric structures. In compounds with a stoichiometric B2 structure, vacancies and anti-site defects can also be combined to form triple defects. When the composition deviates from the stoichiometric ratio, the anti-site atoms play a main role. For ordered B2 phases with some substitution barriers, anti-site defects can act as a bridge to establish low-energy sequences to promote vacancy transitions. A bound pair of vacancies can mediate the diffusion of the two components through the next-nearest-neighbor jumps [24]. For the Ni-rich TiNi alloy used in this paper, the dominant diffusion mechanism is likely to be the anti-structure-bridge mechanism.

The XRD patterns of the Cu-TiNi composites are shown in Fig. 4. The XRD pattern of the Cu-1% TiNi composite does not show the characteristic peak of TiNi due to the very low TiNi content. As the volume percentage of TiNi increases, the characteristic TiNi peak appears and its intensity gradually increases. Fig. 4(b) shows an enlarged partial view of the XRD pattern of the Cu-15% TiNi composite. It is noted that, besides the diffraction peaks of Cu (PDF#04-007-7909) and TiNi (PDF#97-010-5413) phases, the diffraction peaks of a new phase (CuNi)Ti (PDF#97-062-8583) are also visible. The (CuNi)Ti phase belongs to the tetragonal crystal system, with the space group of I4mmm and the lattice constants of a=b=0.312 nm and c=0.7965 nm. The composition of the new phase is consistent with the EPMA results in Fig. 3. It is therefore safe to presume that the diffusion layer at the edge of the TiNi particle (Fig. 3) is the (CuNi)Ti phase.

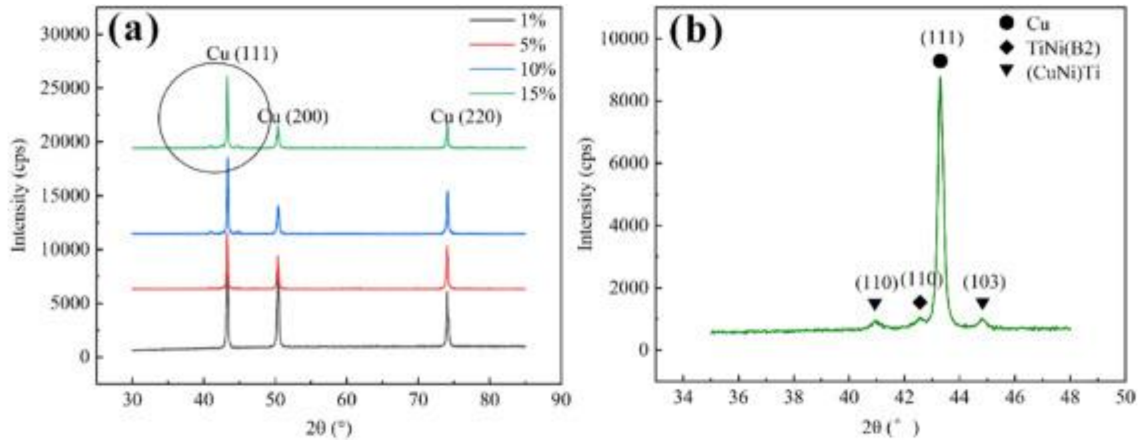

Fig. 4. (a) XRD patterns of Cu-TiNi composites with different TiNi percentages; (b) detailed pattern for Cu-15% TiNi composite in the range of 2θ= 35°-48°.

The appearance of the new (CuNi)Ti phase is consistent with the work of F.J.J et al. [25] who produced the (CuNi)Ti phase through a Cu-TiNi diffusion couple method. F.J.J et al. fabricated Cu-TiNi diffusion couples by solid resistance welding and heated the couples in sealed evacuated silica capsules at different temperatures of 800°C and 870°C for times varying between 16 h and 900 h. A single-phase layer was developed and its structure type was found to be Tetr. $MoSi_2$-type with the lattice parameters a=0.309-0.314 nm, c=0.7965-0.800 nm, c/a=2.546-2.584 [25]. The (CuNi)Ti phase was found to have a fixed structure with a varying composition.

The inverse pole figure (IPF) maps, distribution of grain diameter, IPF distribution along the extrusion direction (ED) of Cu-15% TiNi composites were shown in Fig. 5, where the white arrows represent the extrusion direction. Fig. 5(a) shows the distribution of TiNi powder in composites. It can be seen from Fig. 5(b) that the Cu matrix grains are elongated along the extrusion direction, and the grain orientations were mainly <111> orientation. Fig. 5(c) shows the distribution of Cu matrix grain diameter. Most of the Cu matrix grain diameter is less than 1 μm, and almost all the grain diameter less than 3 μm. It can be seen from Fig. 5(d) that after hot extrusion, the Cu matrix has major <111> + minor<001> fiber textures. In previous study of extrusion of pure Cu, this texture component was attributed to dynamic recrystallization, and the <111> fiber texture is known as the ultimate extrusion texture of FCC metals [26], [27], [28], [29].

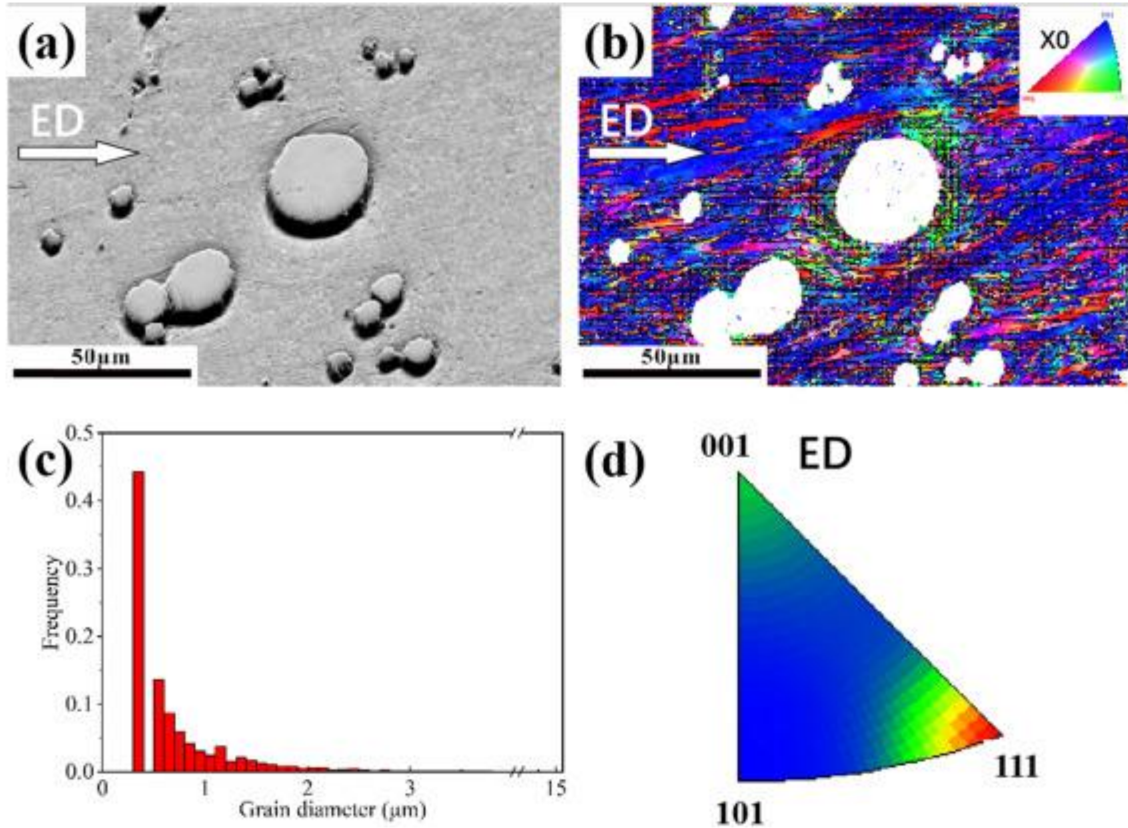

Fig. 5. EBSD data of Cu matrix in Cu-15% TiNi composites: (a) SEM image; (b) IPF map; (c) distribution of grain diameter; (d) IPF distribution along the extrusion direction (ED).

3.2. Analysis of Cu-TiNi Interface

The TEM images and the selected area electron diffraction patterns of the composite Cu-15% TiNi are shown in Fig. 6. Fig. 6(a) shows the full image of the interface region between the Cu matrix and a TiNi particle. There is a high density of dislocations in the Cu matrix near the interface, a large number of which are entangled to form a dislocation wall (Fig. 6(b)). The large number of dislocations can be attributed to large extrusion deformation and mismatch of the thermal expansion coefficients of Cu and TiNi. The high density of entangled dislocations can improve the mechanical properties of the Cu matrix due to work hardening. Area 2 in the Cu matrix shows small Cu grains (around 400 nm) and no dislocation defects, suggesting dynamic recrystallization occurred during the extrusion process. The nano-sized grains can also improve the mechanical properties of the Cu matrix due to Hall-Petch strengthening. Area 3 at the interface shows the presence of the Ni_2Ti_4O phase, which can be inferred by combining the

electron diffraction pattern shown in Fig. 6(e) and the distributions of elements shown in Fig. 6(g). Ni_2Ti_4O is a common oxide in Ti_2Ni alloys [18]. A small amount of Ti_2Ni may be formed during the preparation of TiNi powder [18]. Ni_2Ti_4O found in area 3 was likely generated by the oxidation of Ti_2Ni during storage of the TiNi powder. Ni_2Ti_4O belongs to the cubic crystal system, FD3m space group, with lattice constant a=1.1328 nm. It has a large face-centered cubic unit cell and can be regarded as eight cubic sub-cells. This type of structure can accept a variable number of oxygen atoms without significantly changing the structure [30]. The selected area electron diffraction pattern in area 4 confirms the formation of the (CuNi)Ti phase at the interface, which is consistent with the XRD results. There are no visible dislocations inside the TiNi particle, suggesting that the TiNi particles do not undergo large plastic deformation during the hot press sintering and hot extrusion process.

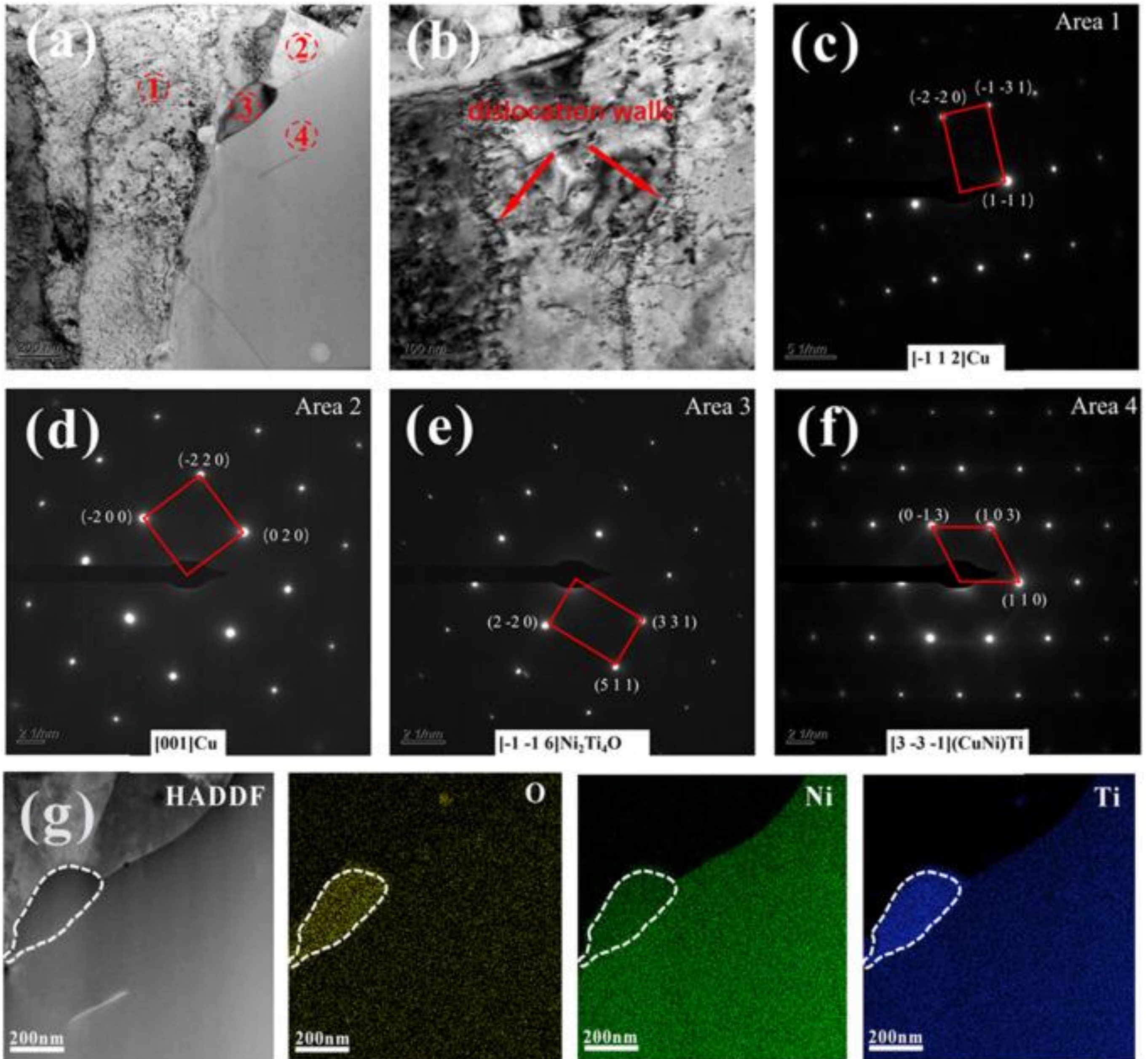

Fig. 6. TEM micrographs in interface region between TiNi particle and Cu matrix (15% TiNi). (a) Full image of interface; (b) Cu matrix; electron diffraction patterns of selected areas (marked with red circles) indexed as: (c) Cu [-1 1 2] in area 1; (d) Cu [0 0 1] in area 2; (e) Ni_2Ti_4O [0 -1 0] in area 3; (f) (CuNi)Ti [3–3–1] in area 4; (g) distributions of elements in area 3.

The high-resolution transmission electron microscopy (HRTEM) image of the interface between the Cu matrix and the TiNi particle in the Cu-15% TiNi composite, and its Fourier transforms are shown in Fig. 7. The HRTEM image (Fig. 7a) shows that there is a clear interface between the Cu matrix (light area) and the (CuNi)Ti (dark area), generated by diffusion of

Cu atoms into TiNi. Its fast Fourier transform (FFT) in Fig. 7(b) shows that there exists an orientation relationship between Cu and (CuNi)Ti. There is also an amorphous layer of about 2 nm thickness formed at the Cu/TiNi interface (Fig. 7c), which has a direct influence on the strength of the interfacial bonding [31]. From Fig. 7(d), the inverse fast Fourier transform (IFFT) of Fig. 7(c), it can be clearly seen that there is a $(111)_{Cu}\|(103)_{(CuNi)Ti}$ orientation relationship between the Cu matrix and the (CuNi)Ti layer. The relationship is a semi-coherent one and the angle between these two crystal planes is about 18.7°. The degree of lattice mismatch at the interface can be calculated by the following formula [32]:

$$\delta = 2(d_{Cu}/cos\theta - d_{(CuNi)Ti}\ )/(d_{Cu}/cos\theta + d_{(CuNi)Ti}) \qquad (2)$$

where θ is the orientation included angle, d_{Cu} and d_{CuNiTi} are the crystal plane spacing of Cu and (CuNi)Ti, respectively. Given $d_{Cu(111)}$ = 0.208 nm and $d_{CuNiTi(103)}$ = 0.202 nm, according to the standard PDF card, and the orientation included angle of 18.7°, the degree of lattice mismatch at the interface is calculated to be 0.025. To maintain the semi-coherent relationship, edge dislocations periodically appear in the (CuNi)Ti phase at the interface, as shown in Fig. 7(d).

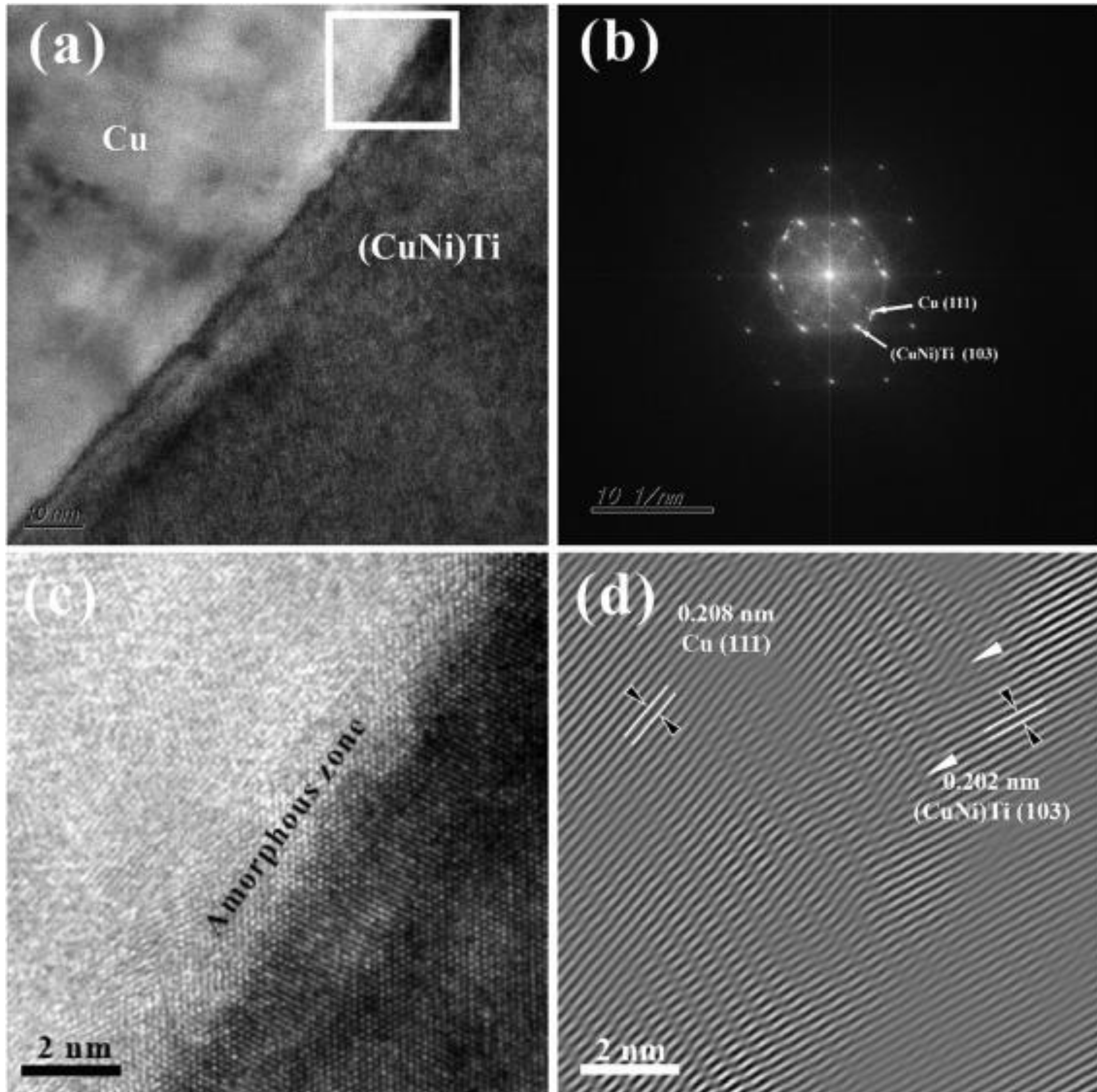

Fig. 7. (a) HRTEM image of Cu/TiNi interface (15% TiNi); (b) FFT; (c) enlarged image of the marked area; (d) IFFT.

The structural development at the interface can be described as follows. As temperature rises during the hot pressing sintering process, Cu atoms diffuse into the TiNi alloy particle, forming a (CuNi)Ti shell around the particle. Cu further nucleates and grows on the surface of the solid (CuNi)Ti particle. At the nucleation stage, a layer of Cu atoms is first formed on the (CuNi)Ti surface. The first crystallized array should have the close-packed crystal orientation and the first crystallized plane the close-packed crystal plane, according to the lowest energy principle [33]. For Cu, the close-packed plane is (111), which is crystallized preferentially. If the interplanar spacing of the (CuNi)Ti surface is close to that of the Cu (111) crystal plane, Cu will crystallize on the (CuNi)Ti surface and grows. The interplanar spacing of

the (103) plane of (CuNi)Ti is the closest to the interplanar spacing of Cu (111) with a difference of only 0.006 nm, hence the $(111)_{Cu}\|(103)_{(CuNi)Ti}$ orientation relationship. Mismatch of the interface is compensated by edge dislocations, resulting in a semi-coherent interface.

3.3. Effect of TiNi content on properties of Cu-TiNi composites

The effects of TiNi volume percentage on the thermal expansion coefficient (room temperature - 100°C), hardness and compressive strength of the composites are shown in Table 2. Increasing volume percentage of TiNi leads to a significant decrease in the thermal expansion coefficient of the Cu-TiNi composite (e.g., 14.11×10^{-6} /K for the Cu-15% TiNi composite), highlighting the role of TiNi alloy particles in enhancing the dimensional stability of the pure Cu matrix. Given that the thermal expansion coefficient (room temperature -100 °C) of pure Cu and TiNi are about 16.7×10^{-6} /K [34] and 13.5×10^{-6} /K [35], respectively, The decrease of the thermal expansion coefficients of the Cu-TiNi composites can mainly be attributed to the restriction of the reinforcement on the matrix through the matrix-reinforcement interface. Increasing TiNi content increases the Cu-TiNi interface and therefore the restraint effect. the thermal expansion coefficients of the composites are well below those predicted by rule of mixture. It can be attributed to the following two factors: (1) Original pore defects exist in TiNi particles can be regarded as zero thermal expansion. (2) <111> fiber texture along the extrusion could lower the thermal expansion of Cu matrix. Thermal expansion is an elastic dilatation caused by the thermal forces, which could be related to the elasticity modulus of materials. For FCC metals, the <111> direction has the maximum value of directional elasticity modulus and has the lowest expansion correspondingly [36]. Similar phenomenon has also been reported by Tae-Hyuk Lee et al. [37].

Table 2. Thermal expansion coefficient, hardness and compressive yield strength of the Cu-TiNi composites.

Volume percentage of TiNi	**1%**	**5%**	**10%**	**15%**
Thermal expansion coefficient, 10^{-6}/K	14.82	14.63	14.43	14.11
Average hardness, Hv	77.5	129.2	147.3	154.4
Compressive yield strength, MPa	194.0	323.1	414.2	460.0

The Vickers hardness of the composites increases significantly with increasing the volume percentage of TiNi. This is because adding TiNi particles to the Cu matrix enhances the resistance to local plastic deformation. The reinforcing particles confine the deformation of the matrix to a local area by restricting the slip of dislocations, leading to increasing residual stress and increased hardness of the composites [38]. In addition, the diffusion of Ti and Ni into the Cu matrix, as shown by the EPMA results, produces a solid solution strengthening effect. The hardness of the Cu matrix is increased, thereby increasing the hardness of the composites.

The compressive yield strength of the Cu-TiNi composites increases with increasing TiNi content, being 194.0, 323.1, 414.2 and 460.0 MPa when 1%, 5%, 10% and 15% of TiNi is added, respectively. TiNi particles hinder the slip of dislocations during the deformation of the Cu matrix and thus improve the compressive strength of the composites [39]. Effective strengthening of the composites requires uniform distribution of the TiNi particles in the Cu matrix and good interfacial bonding at the Cu-TiNi interface. The fact that the Cu-TiNi composite specimens did not fracture and showed good plasticity during compression demonstrates good interfacial bonding between the TiNi reinforcement and the Cu matrix. More specifically, the increase in the compressive strength of the composites can be attributed to the combined effects of load transfer, mismatch of thermal expansion coefficient and elastic modulus, and solid solution strengthening, which can be quantitatively evaluated as follows.

Under compression, the load is transferred from the Cu matrix to the TiNi particles. The TiNi particles will bear a higher proportion of the load than its volume percentage, due to higher elastic modulus, and limit the deformation

of the matrix. The contribution of the load transfer effect to strength can be expressed by [40]:

$$\Delta\sigma_l = v_p\sigma_m\left[\frac{(L+t)A}{41}\right] \quad (3)$$

where v_p is the volume fraction of the reinforcing particles, σ_m is the yield strength of the matrix, L and t are the particle sizes parallel to and perpendicular to the loading direction, respectively, and A is a geometric constant.

When the Cu-TiNi composites are cooled down from the hot extrusion temperature, stresses will be generated due to the differences in thermal expansion coefficient and elastic modulus between TiNi and Cu. As a consequence, a large number of dislocations will be generated around the TiNi particles. The geometrically necessary dislocation densities produced by the differences in thermal expansion coefficient and elastic modulus are [41]:

$$\rho_{CTE} = \frac{A\Delta\alpha\Delta T v_P}{bd_p(1-v_p)} \qquad \rho_{EM} = \frac{6v_p}{\pi d_p^3}\varepsilon \quad (4)$$

where ρ_{CTE} and ρ_{EM} are the geometrically necessary dislocation density due to thermal expansion coefficient and elastic modulus, respectively, A is a geometric constant, $\Delta\alpha$ is the difference in thermal expansion coefficient, ΔT is the difference between the hot extrusion and room temperatures, b is Burgers vector (m), d_p is particle diameter, ε is the uniform deformation. The contribution of the mismatch strengthening can be expressed by [42]:

$$\Delta\sigma_c = \sqrt{3}\beta Gb\left(\sqrt{\rho_{CTE}} + \sqrt{\rho_{EM}}\right) \quad (5)$$

where β is a constant and G is the shear modulus of the Cu matrix.

Ti and Ni diffuse into the Cu matrix and the dissolved elements cause solid solution strengthening of the Cu matrix. The improvement of strength by solid solution strengthening can be calculated by:

$$\Delta\sigma_s = \sum G\delta^{3/2}\sqrt{\frac{X_a}{3}} \quad (6)$$

where δ is the lattice distortion factor of the matrix caused by the solid solution elements and X_a is the atomic percentage of the solid solution elements.

4. Conclusions

(1). Cu-TiNi composites with uniform microstructure and good mechanical properties were prepared by vacuum hot pressing sintering and hot extrusion. Diffusion of elements occurred at the interface between the Cu matrix and the TiNi particles during the preparation process, with the depth of Cu diffusion to the TiNi particles reaching 15 μm, leading to the formation of a new (CuNi)Ti phase. The Cu matrix has major <111> + minor <001> fiber textures after hot extrusion.

(2). The TiNi particles are well bonded to the Cu matrix. A semi-coherent interface form between the copper matrix and the (CuNi)Ti phase, with the orientation relationship of $(111)_{Cu}\|(103)_{(CuNi)Ti}$ and the angle between the two crystal planes of 18.7°. There are a large number of dislocations inside the Cu matrix near the interface.

(3). Increasing TiNi content decreased the thermal expansion coefficient and increased the Vickers hardness and compressive yield strength of the Cu-TiNi composites. With 15 vol% of TiNi, the thermal expansion coefficient of the composite decreased to 14.11×10^{-6} /K, the Vickers hardness increased to 154.4 Hv, and the compressive yield strength increased to 460.0 MPa. The increases in the mechanical properties can be attributed to the combined effects of load transfer, mismatch of thermal expansion coefficient and elastic modulus, and solid solution strengthening.

Acknowledgements

The authors acknowledge the financial support by the National Natural Science Foundation of China (51974375), Technology Research Program of Ningbo, China (No. 2019B10088), and grants from the Project of Innovation-Driven Plan and the Project of State Key Laboratory of Powder Metallurgy, Central South University, Changsha, China.

References

[1] M.S. Abd-Elwahed, A. Wagih, I.M.R. Najjar, **Correlation between micro/nano-structure, mechanical and tribological properties of copper-zirconia nanocomposites,** Ceramics International, 46 (2020), pp. 56-65, 10.1016/j.ceramint.2019.08.230

[2] Y.Q. Qin, Y.C. Wu, X.M. Huang, Y. Wang, J.W. Cui, Y. Hong, Y.C.Zheng, **Effect of heat treatment on conductivity of Cu-1.0Cr-0.12Zr alloy,** Advanced Materials Research, 1061-, 1062 (2015), pp. 7-12, 10.4028/www.scientific.net/AMR.1061-1062.7

[3] B. Huang, Y. Hishinuma, H. Noto, T. Muroga, **Mechanochemical processing of Cu-Y2O3 alloy by MA-HIP for heat sink materials application,** Fusion Engineering & Design, 140 (2019), pp. 33-40, 10.1016/j.fusengdes.2019.01.133

[4] R. Prieto, J.M. Molina, J. Narciso, E. Louis, **Fabrication and properties of graphite flakes/metal composites for thermal management applications,** Scripta Materialia, 59 (2008), pp. 11-14, 10.1016/j.scriptamat.2008.02.026

[5] R. Couturier, D.D. Ucret, P. Merle, J.P. Disson, P. Joubert, **Elaboration and characterization of a metal matrix composite: Al/AlN,** Journal of the European Ceramic Society, 17 (1997), pp. 1861-1866, 10.1016/S0955-2219(97)87873-9

[6] B.G. Kim, S.L. Dong, D.P. Su, **Effects of thermal processing on thermal expansion coefficient of a 50 vol.% SiCp/Al composite,** Materials Chemistry & Physics, 72 (2001), pp. 42-47, 10.1016/S0254-0584(01)00306-6

[7] K. Chu, Z. Liu, C. Jia, H. Chen, X. Liang, W. Gao, W. Tian, H. Guo, **Thermal conductivity of SPS consolidated Cu/diamond composites with Cr-coated diamond particles,** Journal of Alloys & Compounds, 490 (2010), pp. 453-458, 10.1016/j.jallcom.2009.10.040

[8] A. Gruzdkov, S. Krivosheev, Y. Petrov, A. Razov, A. Utkin, **Martensitic inelasticity of TiNi-shape memory alloy under pulsed loading,** Materials Science & Engineering A, 481-482 (2008), pp. 105-108, 10.1016/j.msea.2007.03.113

[9] Y. Furuya, A. Sasaki, M. Taya, **Enhanced mechanical properties of TiNi shape memory fiber/Al matrix composite,** Materials Transactions, 34 (1993), pp. 224-227, 10.2320/matertrans1989.34.224

[10] Y. Furuya, A. Shimamoto, M. Taya, **Enhancement of mechanical properties of TiNi fiber composites by shape memory effect, US-Japan Workshop on Smart,** Materials and Structures (1996), pp. 65-74, https://doi.org/WOS:000078856600008

[11] D.R. Ni, Z.Y. Ma, **Shape memory alloy-reinforced metal-matrix composites: A review,** Acta Metallurgica Sinica, 27 (2014), pp. 739-761, 10.1007/s40195-014-0164-x

[12] J.-F. Li, Z.-Q. Zheng, X.-W. Li, Z.-W. Peng, **Application of shape memory alloy TiNi in low thermal expansion copper composites,** Materials & Design, 30 (2009), pp. 314-318, 10.1016/j.matdes.2008.04.077

[13] T. Aydogmus, **Processing of interpenetrating Mg–TiNi composites by spark plasma sintering,** Materials Science and Engineering: A, 624 (2015), pp. 261-270, 10.1016/j.msea.2014.11.092

[14] I.-S. Ahn, S.-Y. Bae, Y.-Y. Kim, **Properties of Al/TiNi composite using porous TiNi fabricated by a self-propagating high temperature synthesis method,** Metals and Materials International, 10 (2004), pp. 39-44, 10.1007/BF03027362

[15] Y.C. Park, Y.J. Jo, S.H. Baek, Y. Furuya, **Fatigue design curve of a TiNi/Al shape memory alloy composite for aircraft stringer design,** Smart Materials & Structures, 18 (2009), Article 055009, 10.1088/0964-1726/18/5/055009

[16] Y.C. Park, J.H. Kang, J.K. Lee, G.C. Lee, Y. Furuya, **Effect of cold rolling on fatigue crack propagation of TiNi/Al6061 shape memory composite,** Smart Materials and Structures, 16 (2007), pp. 982-988, 10.1088/0964-1726/16/4/005

[17] Y. Freed, J. Aboudi, **Micromechanical prediction of the two-way shape memory effect in shape memory alloy composites,** International Journal of Solids and Structures, 46 (2009), pp. 1634-1647, 10.1016/j.ijsolstr.2008.12.004

[18] K. Otsuka, X. Ren, **Physical metallurgy of Ti–Ni-based shape memory alloys** Progress in Materials Science, 50 (2005), pp. 511-678, 10.1016/j.pmatsci.2004.10.001

[19] R.R. Thorat, D.D. Risanti, D. San Martín, G. Garces, P.E.J.Rivera D.íaz del Castillo, S. van der Zwaag, **On the transformation behaviour of NiTi particulate reinforced AA2124 composites,** Journal of Alloys and Compounds, 477 (2009), pp. 307-315, 10.1016/j.jallcom.2008.11.002

[20] J. Hu, G. Wu, Q. Zhang, P. Kang, Y. Liu, **Microstructure of multilayer interface in an Al matrix composite reinforced by TiNi fiber,** Micron, 64 (2014), pp. 57-65, 10.1016/j.micron.2014.02.014

[21] T. Xiao, Z. Li, Z. Xiao, X. Zhang, W. Qiu, Y. Wang, X. Guo, Q. Lei, **Fabrication of a Cu/TiNi composite with high air-tightness and low thermal expansion,** JOM, 72 (2019), pp. 883-888, 10.1007/s11837-019-03930-w

[22] L. Ning, S. Tao, X. Junxiang, **Diffusion mechanism of explosive welding interface between memory alloy Ni50Ti50 and Cu,** Rare Metal Materials and Engineering, 47 (2018), pp. 324-328, https://doi.org/1002-185X(2018)10-3238-05

[23] M. Mohri, M. Nili-Ahmadabadi, S. Flege, **Diffusion evaluation of Cu in NiTi Bi-layer thin film interface,** Journal of Alloys and Compounds, 594 (2014), pp. 87-92, 10.1016/j.jallcom.2014.01.068

[24] P. Heitjans, J. Karger (Eds.), Diffusion in Condensed Matter: Methods, Materials, Models (2nd ed.), Springer, Berlin (2005), 10.1007/3-540-30970-5

[25] F.J.J. van Loo, G.F. Bastin, A.J.H. Leenen, **Phase relations in the ternary Ti-Ni-Cusystem at 800 and 870 degrees C,** Journal of the Less Common Metals, 57 (1978), pp. 111-121, 10.1016/0022-5088(78)90167-4

[26] Dong Nyung, Lee, **The evolution of recrystallization textures from deformation textures,** Scripta Metallurgica et Materialia, 32 (10) (1995), pp. 1689-1694, 10.1016/0956-716X(95)00256-U

[27] N. Pardis, C. Chen, R. Ebrahimi, L.S. Toth, C.F. Gu, B. Beausir, L. Kommel, **Microstructure, texture and mechanical properties of cyclic expansion-extrusion deformed pure copper,** Materials Science and Engineering A, 628 (mar.25) (2015), pp. 423-432, 10.1016/j.msea.2015.01.003

[28] W.R. Hibbard, **Deformation texture of drawn face centered cubic metal wires,** Trans. AIME, 77 (1950), pp. 581-585

[29] H. Ahlborn, G. Wassermann, **Einfluß von Verformungsgrad und -temperatur auf die Textur von Silberdrähten,** International Journal of Materials Research, 54 (1) (1963), pp. 1-6, 10.1515/ijmr-1963-540101

[30] M.H. Mueller, H.W. Knott, **The crystal structures of Ti2Cu, Ti2Ni, Ti4Ni2O, and Ti4Cu2O,** Trans AIME, 227 (1963)

[31] M. Liang, P. Wang, X. Xu, G. Jiao, C. Li, P. Zhang, **Interface structure of high strength and high conductivity Cu-Nb microcomposites,** Rare Metal Materials and Engineering, 46 (2017), pp. 1288-1292, https://doi.org/1002-185X(2017)05-1288-05

[32] K.H. Lee, S.I. Hong, **Interfacial structure of nanostructured Cu-Nb filamentary composite fabricated by the bundling and drawing process,** Philosophical Magazine Letters, 84 (2004), pp. 515-523, 10.1080/09500830412331298877

[33] J. Longtao, Z. Min, W. Gaohui, Z. Qiang, **Aging behavior of sub-micron Al2O3P/2024Al composites,** Materials Science and Engineering: A, 392 (2005), pp. 366-372, 10.1016/j.msea.2004.09.048

[34] S. Gao, N. Zhao, Q. Liu, Y. Li, G. Xu, X. Cheng, J. Yang, **Sc2W3O12/Cu composites with low thermal expansion coefficient and high thermal conductivity for efficient cooling of electronics,** Journal of Alloys and Compounds, 779 (2019), pp. 108-114, 10.1016/j.jallcom.2018.11.131

[35] X. Shi, H. Lian, R. Qi, L. Cui, N. Yao, **Preparation and properties of negative thermal expansion Zr2P2WO12 powders and Zr2P2WO12/TiNi composites,** Materials Science and Engineering: B, 203 (2016), pp. 1-6, 10.1016/j.mseb.2015.10.005

[36] E. Balikci, A. Raman, R.A. Mirshams, **Microstructure and texture effect on the thermal expansion of a variously aged polycrystalline superalloy IN738LC,** Metallurgical and Materials Transactions A, 30 (11) (1999), pp. 2803-2808

[37] T.H. Lee, Y.J. Lee, K.T. Park, H.G. Jeong, J.H. Lee, **Mechanical and asymmetrical thermal properties of Al/Cu composite fabricated by repeated hydrostatic extrusion process,** Metals and Materials International, 21 (2) (2015), pp. 402-407

[38] M.P. Reddy, V. Manakari, G. Parande, R.A. Shakoor, A.M.A. Mohamed, M. Gupta, **Structural, mechanical and thermal characteristics of Al-Cu-Li particle reinforced Al-matrix composites synthesized by microwave sintering and hot extrusion,** Composites Part B: Engineering, 164 (2019), pp. 485-492, 10.1016/j.compositesb.2019.01.063

[39] S.M.K. Surappa, **Synthesis of fly ash particle reinforced A356 Al composites and their characterization,** Materials Science & Engineering A, 480 (2008), pp. 117-124, 10.1016/j.msea.2007.06.068

[40] V.C. Nardone, K.M. Prewo, **On the strength of discontinuous silicon carbide reinforced aluminum composites,** Scripta Metallurgica, 20 (1) (1986), pp. 43-48, 10.1016/0036-9748(86)90210-3

[41] A. Sanaty-Zadeh, P.K. Rohatgi, **Corrigendum to: Comparison between current models for the strength of particulate-reinforced metal matrix nanocomposites with emphasis on consideration of Hall–Petch effect,** 302-302, Materials Science and Engineering: A, 551 (2012), 10.1016/j.msea.2012.04.039

[42] R.E. Smallman, A. Ngan, **Physical properties,** Physical Metallurgy & Advanced Materials Engineering, 22 (2007), pp. 239-288, 10.1007/BF00445201